Electronic Supplementary Material (ESI) for Energy & Environmental Science.
This journal is © The Royal Society of Chemistry 2026

Supporting Information

A synergistic dual additive strategy for constructing gradient hydrophobic interfaces toward ultrastable aqueous zinc metal anodes

Zongpu Xia,[a†] Jingyi Ding,[ad†] Sicheng Yang,[a] Qiaoli Zhang,[b] Yiwei Yuan,[b] Chengyuan Peng,[a] Junrong Luo,[a] Junhao Du,[a] Fei Ye,[a] Yanzhi Ai,[a] Yue Wang,[e] Xinxiang Zhang,[a] Wen Liu[bc] and Jitao Chen*[a]*

[a] College of Chemistry and Molecular Engineering, Peking University, Beijing 100871, China

[b] College of Chemistry, Beijing University of Chemical Technology, Beijing 100029, China

[c] State Key Laboratory of Chemical Resource Engineering, Beijing University of Chemical Technology, Beijing 100029, China

[d] Suzhou Laboratory, Suzhou 215123, China

[e] Institute of NBC Defense, PLA Army, Beijing 102205, China

[†] These authors contributed equally to this work.

*Corresponding Author: chenjitao@pku.edu.cn, wenliu@mail.buct.edu.cn

Experimental Section

Materials:

Zn−foil (10 μm and 30 μm), Cu−foil (50 μm) were purchased from Sinopharm Chemical Reagent Co., Ltd. $ZnSO_4·7H_2O$ (>99.0%), $KMnO_4$ (>99.0%), $MgSO_4$ (>99.5%), $MnSO_4·H_2O$ (>99.0%), benzyl acetone (BZA), ethanol (EtOH), N−methyl−2−pyrrolidone (NMP) were purchased from Aladdin Co., Ltd. polyvinylidene fluoride (PVDF) and acetylene black (AB) were purchased from Suzhou DodoChem Technology Co., Ltd.

The polished Zn electrode was obtained by removing the passivation layer using an abrasive paper. All other reagents were analytical grade (AR) and used directly without further purification. Deionized water (DI) was used to prepare all aqueous electrolytes.

Preparation of Electrolyte:

Aqueous electrolyte was prepared using $ZnSO_4·7H_2O$, $MgSO_4$, BZA, EtOH and DI based on molar ratio. Specifically, $ZnSO_4·7H_2O$ (28.76 g, 0.1 mol) was added to 50 mL of DI, followed by 0, 0, 0.25, 0.25 mmol (0, 0, 36.54 mg, 36.54 mg, respectively) of BZA, 0, 1.000 mL, 0, 1.000 mL EtOH, and the mixture was stirred for 0.5 h. Then the solution was sonicated for 15 minutes to give a clarified, colorless and transparent electrolyte, which was noted as ZS, ZE, ZB, ZEB. The preparation procedure for the $MgSO_4$ electrolyte used in LSV testing is as follows: $MgSO_4$ (12.04 g, 0.1 mol) was added to 50 mL of DI, followed by identical steps to those described above.

Preparation of δ−MnO_2 Cathode:

6.0 mM $KMnO_4$ and 1.0 mM $MnSO_4·H_2O$ were dispersed in 30.0 mL DI at 25 °C. The mixture was then transferred to a Teflon-lined autoclave and heated at 160 °C for 12 h. The obtained product was collected by filtration, washed with DI and ethanol, and ultimately dried at 80 °C.

The cathode was fabricated by mixing the δ−MnO_2 powder, AB, and PVDF with a weight ratio of 70:15:15 using NMP as solvent. The mixture slurry was printed on hydrophilic carbon circular discs and then transferred to a vacuum oven drying at 60 °C for 24 h. The loading mass of cut disc of electrodes is all within the scope of 1.2~1.8 mg along with a diameter of 0.8 cm.

Characterization:

The Nuclear Magnetic Resonance (NMR, Bruker-400), Fourier Transform Infrared (FTIR, Thermo Nicolet iS50), and Sum Frequency Generation Vibrational Spectroscopy (SFG, EKSPLA SFG-073) were employed to analyze the element and surface chemistry of the samples. Zn foils were characterized with X-ray Diffraction (XRD, PANalytical X-Pert3 Powder, Cu-K_α radiation), Scanning Electron Microscopy (SEM, Hitachi S-4800), X-ray Photoelectron Spectroscopy (XPS, Kratos Analytical Ltd. AXIS Supra), and (EBSD, Bruker QUANTAX eFlashFS). It is necessary to clarify that the surface of the EBSD sample was treated with argon ion polishing. The ion beam

energy was set at 6 kV, the ion gun angle at 3°, and the processing time was 20 minutes. The in-situ optical microscope images, videos, and contact angles were obtained on an electron microscope (WYT-GTY, Viyee Photoelectric Devices (Tianjin) Co., Ltd., China) by using a homemade in-situ optical electrochemical cell.

Electrochemical Measurements:

Electrochemical performance was tested using CR2032−type coin cells. Whatman GF/D glass microfiber was employed as the separator. The electrolyte volume in each coin cell was 0.1 mL. Cyclic voltammetry (CV) measurements were conducted with an electrochemical workstation (Autolab, China) between 1.0 and 1.8 V for Zn||δ−MnO_2 full cells and between −1.015 and −0.995 V for Zn||Zn symmetric cells. Linear scanning voltammetry (LSV), Nyquist curves, chronoamperometry (CA) curves, and electrochemical impedance spectroscopy (EIS) were also performed on the Autolab. The cycling stability of the Zn anode was tested using Zn||Zn symmetric cells. Depth of discharge (DOD) testing used ultra-thin zinc foil (10 μm), while other coin cells used thick zinc foil (30 μm). Coulombic efficiency (CE) was determined using Zn||Cu asymmetric cells. Zn||δ−MnO_2 full cells were assembled to evaluate the practical application value of the cells at current densities of 30.8 mA g^{-1}, 92.4 mA g^{-1}, 154 mA g^{-1}, 308 mA g^{-1}, 924 mA g−1, and 1.54 A g^{-1}. The Blue Power Test System (Land−2001A, China) was used to perform charge/discharge tests. Each pouch-type Zn||δ−MnO_2 full cell consisted of one 4.2×4.2 cm^2, 10 μm Zn foil as the anode, one 4.4×4.4 cm^2 GF/D glass fiber as the separator, and one 4.0×4.0 cm^2 carbon paper loaded with 7−9 mg cm^{-2} of δ−MnO_2 as the cathode.

Desolvation energy barrier (E_a):

The de−solvation process of Zn^{2+} is considered to be the rate−limiting process for the deposition of zinc at the anode. It is usually analyzed using the activation energy (E_a) obtained from the Arrhenius equation law.

$$\frac{1}{R_{ct}} = A \exp(-\frac{E_a}{RT})$$

where R_{ct} is the charge−transfer resistance, A is the frequency factor, R is the gas constant, and T is the absolute temperature.

Zn−ion transference number:

The Zn^{2+} transference number ($t_{Zn^{2+}}$) was measured by Bruce–Vincent method.

$$t_{Zn^{2+}} = \frac{I_{ss}(\Delta V - I_0 R_0)}{I_0(\Delta V - I_{ss} R_{ss})}$$

where ΔV is the applied constant polarization voltage (20 mV), I_0 and I_{ss} are the initial and steady current, and R_0 and R_{ss} are the initial and steady resistance.

Cyclic voltammetry (CV) b value:

By obtaining the CV curves of the full cell at different scan rates, the relationship curves between the peak current values of each peak and the scan rate are obtained. The b value is calculated through the following formula:

$$I = av^b$$

where I is the peak current, v is the scan rate, a and b are the fitting parameters. The testing was conducted at room temperature.

Cumulative Plated Volumetric Capacity (CPVC):

CPVC eliminates the influence of zinc foil thickness compared to Cumulative Plated Capacity (CPC, unit: Ah cm^{-2}). The calculation method is as follows:

$$CPVC = \frac{CPC}{d_{Zn}} = \frac{CD \times t}{d_{Zn}} \quad (1)$$

where d_{Zn} is the zinc foil thickness, CD is the current density, and t is the test duration. t can be correlated with CD, areal capacity (AC), and the number of cycles (N):

$$CD \times t = 2N \times AC \quad (2)$$

When a battery does not fail during a test (e.g., due to dendrite penetration or electrolyte depletion), its maximum number of cycles (N_{max}) can be predicted based on the depth of discharge (DOD) and average Coulombic efficiency (ACE):

$$N_{max} = \frac{DOD^{-1} - 1}{1 - ACE} \quad (3)$$

The areal capacity (AC) is related to the depth of discharge (DOD) and the zinc foil thickness (d_{Zn}) by the following expression:

$$AC = DOD \times d_{Zn} \times \frac{n_{Zn} \times \rho_{Zn} \times F}{3600 \times M_{Zn}} \quad (4)$$

where n_{Zn} is the number of electrons transferred per Zn atom, ρ_{Zn} is the density of Zn, F is Faraday's constant (96485 C mol^{-1}), 3600 is the unit conversion constant between ampere-hour (Ah) and coulomb (C), and M_{Zn} is the molar mass of Zn. By combining Equations (1), (2), (3), and (4), Equation (5) can be derived, which represents the theoretical maximum CPVC ($CPVC_{max}$) of the battery system:

$$CPVC_{max} = \frac{n_{Zn} \times \rho_{Zn} \times F}{1800 \times M_{Zn}} \times \frac{1 - DOD}{1 - ACE} \quad (5)$$

DFT calculations:

All periodic density functional theory (DFT) calculations were performed using the Quickstep module of CP2K (version 2025.1)[1,2]. The exchange–correlation energy was described by the Perdew–Burke–Ernzerhof (PBE) functional within the generalized gradient approximation (GGA)[3], and core electrons were represented by the Goedecker–Teter–Hutter (GTH) pseudopotentials[4]. Dispersion corrections were included using Grimme's D3BJ method[5,6]. For geometry optimizations, the DZVP-MOLOPT-SR-GTH basis set was employed for all atoms, while single-point energy calculations utilized the TZV2P-MOLOPT-GTH basis set[7]. A plane-wave cutoff energy of 650 Ry was applied in all computations.

The adsorption energy (E_{ads}) between the zinc slab and the molecule was calculated according to the following equation:

$$E_{ads} = E_{total} - E_{mole} - E_{slab}$$

where E_{total}, E_{mole}, and E_{slab} stand for the total energy of the optimized composite system, the energy of the isolated adsorbed molecule, and the energy of the clean zinc slab, respectively.

In this study, the adsorption behaviors of water and organic molecules on the Zn(002), Zn(100), and Zn(101) slabs were compared. Each surface model was constructed as a four-layer zinc slab, with the bottom two layers fixed during structural relaxation. Supercells of 7 × 7, 6 × 5, and 4 × 6 were built for the Zn(002), Zn(100), and Zn(101) slabs, respectively. Brillouin zone sampling was performed using Monkhorst–Pack grids of 4 × 4 × 1, 4 × 2 × 1, and 2 × 4 × 1 for the corresponding surfaces[8].

Prior to analyzing molecular surface electrostatic potentials, geometry optimizations were carried out with Gaussian 16[9] at the B3LYP/6-311G(d,p) level[10], incorporating Grimme's D3BJ dispersion correction. Visualization was conducted using VMD (Visual Molecular Dynamics) software[11].

The generation of CP2K input files and the analysis of molecular surface electrostatic potentials were performed with the Multiwfn 3.8(dev) code[12–14].

Molecular dynamics simulation:

Molecular dynamics (MD) simulations were conducted with GROMACS software[15]. A time step of 1 fs was employed, with a cutoff distance of 1.0 nm for both the van der Waals interactions and electrostatic interactions. The electrostatic interactions were calculated by the particle mesh Ewald method (PME). The nonbonded interaction contains van der Waals (vdW) and electrostatic interactions, which are described by the Equation as follows.

$$E_{LJ}(r_{ij}) = 4\varepsilon_{ij}\left[\left(\frac{\varepsilon_{ij}}{r_{ij}}\right)^{12} - \left(\frac{\varepsilon_{ij}}{r_{ij}}\right)^{6}\right]$$

$$E_c(r_{ij}) = \frac{q_i q_j}{4\pi\varepsilon_0\varepsilon_r r_{ij}}$$

The size of the cubic box is 6.4 × 5.6 × 7 nm^3 (with periodic boundary conditions). The pure system contains one Zn electrode, 280 Zn^{2+}, 280 SO_4^{2-}, and 7000 H_2O. The system 2 contains one Zn electrode, 280 Zn^{2+}, 280 SO_4^{2-}, 300 EtOH, 100 BZA, and 7000 H_2O. The water model was OPC3, and the interaction parameters of various ions and molecules were taken from the GAFF force field. In the NVT simulations, the V-rescale thermostat with a

characteristic time of 2 ns was applied to implement the constant temperature condition. For the production simulations, the simulations were carried out for 30 ns to ensure the system reached equilibrium, and the last 5 ns of the equilibrium state were used for subsequent post-processing analysis.

Supplementary Figures

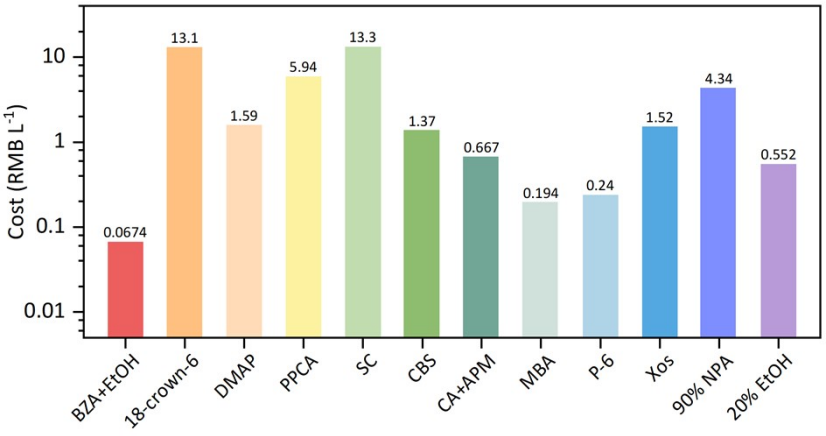

Fig. S1. Unit cost of multifunctional electrolyte formulations.

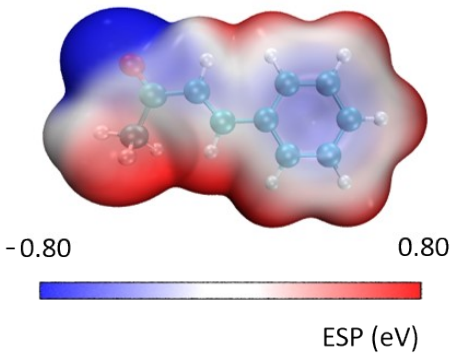

Fig. S2. The electrostatic potential (ESP) of BZA.

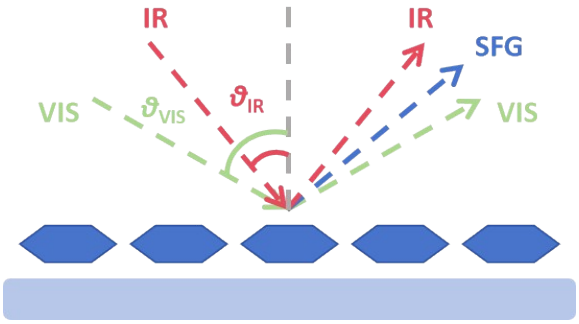

Fig. S3 Schematic diagram of the vibrational sum-frequency generation (VSFG) spectroscopic setup. (λ_{VIS} = 532 nm, ϑ_{VIS} = 60°, ϑ_{IR} = 55°, E_{VIS} = 200 μJ, E_{IR} = 150 μJ).

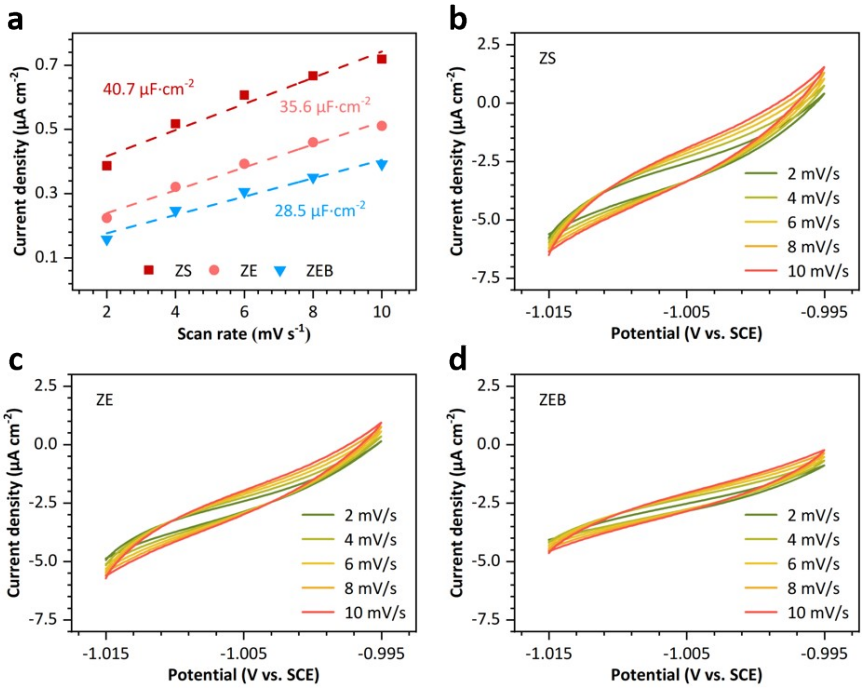

Fig. S4 (a) Fitted double-layer capacitance results; CV curves for (b) ZS, (c) ZE, (d) ZEB.

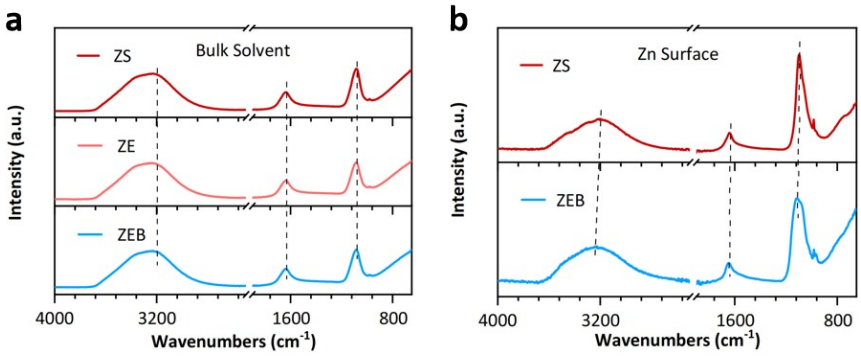

Fig. S5 ATR−FTIR spectra of (a) bulk solution; (b) solution near the Zn surface

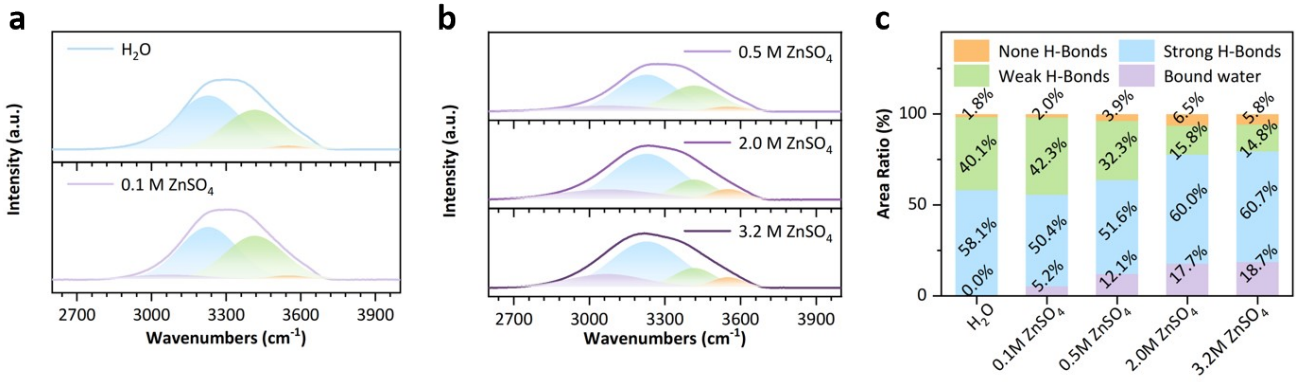

Fig. S6 (a), (b) ATR−FTIR spectra of H_2O and $ZnSO_4$ solutions of different concentrations; (c) Hydrogen bond composition ratios.

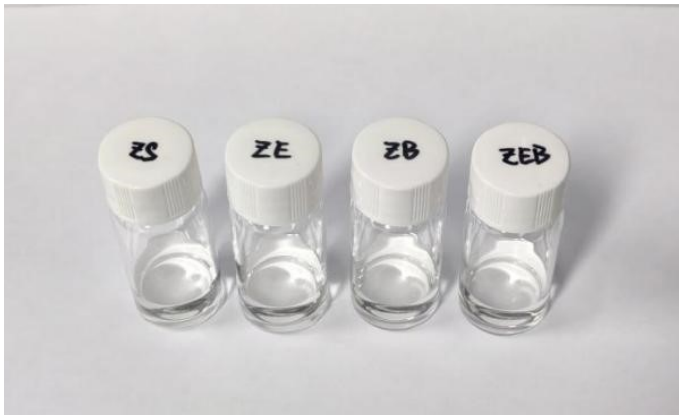

Fig. S7 Schematic diagram of homogeneous electrolytes (ZS is 2 M $ZnSO_4$; ZE is ZS + 2% EtOH; ZB is ZS + 5 mM BZA; ZEB is ZE + 5 mM BZA).

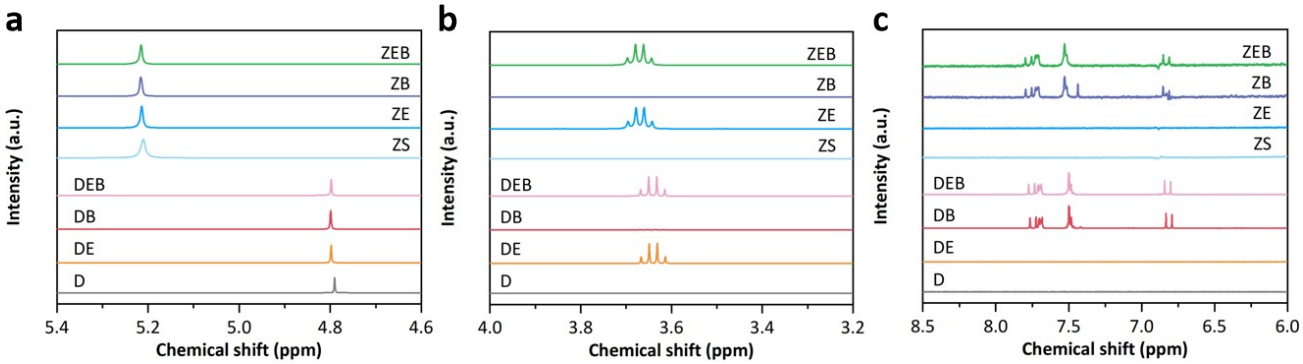

Fig. S8 ^1H NMR spectra of different electrolytes: (a) Water peak; (b) Ethanol $-CH_2-$ peak; (c) BZA peaks (D = D_2O; DE = D_2O+EtOD; DB = D_2O+BZA; DEB = D_2O+EtOD+BZA; ZB = ZS+BZA).

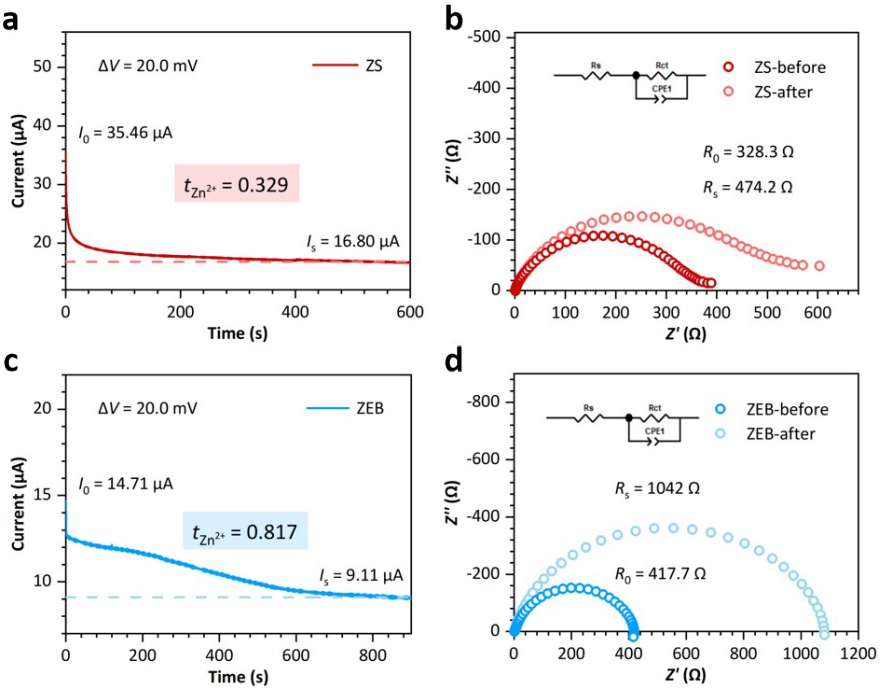

Fig. S9 Zn^{2+} transference number tests: (a),(c) Chronoamperometry (CA) tests; (b),(d) EIS spectra and fitted resistance results before and after activation.

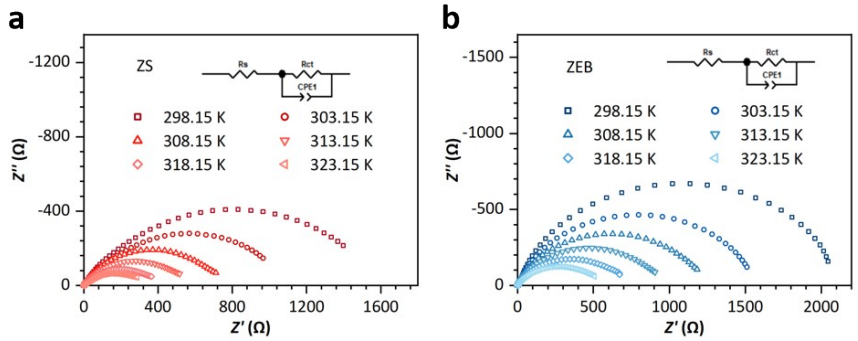

Fig. S10 Raw data for Zn^{2+} desolvation energy: EIS spectra of Zn||Zn symmetric cells at different temperatures using (a) ZS electrolyte; (b) ZEB electrolyte.

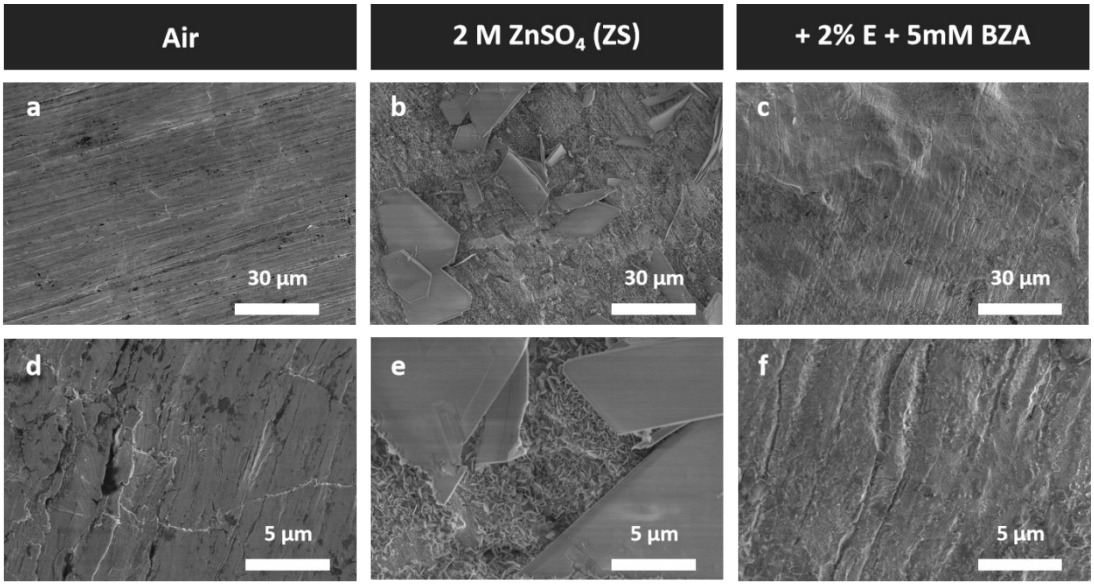

Fig. S11 SEM images of the electrolyte immersion test: Zn foils immersed for 7 days in (a),(d) air; (b),(e) ZS electrolyte; (c),(f) ZEB electrolyte.

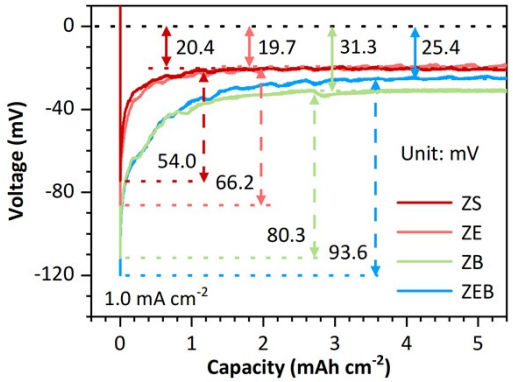

Fig. S12 Voltage−capacity curve tests.

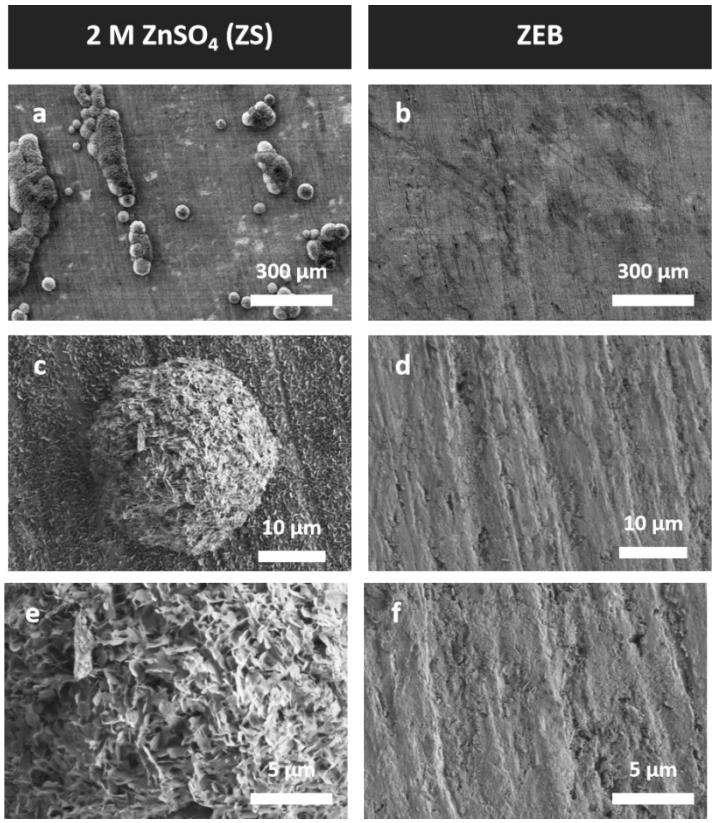

Fig. S13 SEM images of Zn foil surfaces after deposition for 1 h at 10 mA cm^{-2} in (a),(c),(e) ZS electrolyte and (b),(d),(f) ZEB electrolyte.

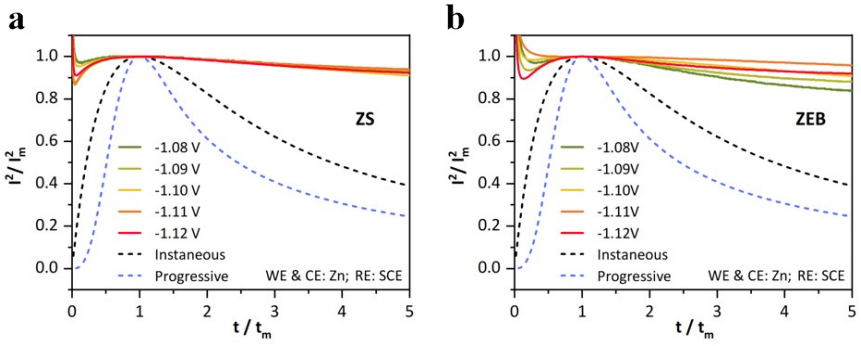

Figure S14. The dimensionless curves of zinc nucleation process in (a) ZS and (b) ZEB electrolytes.

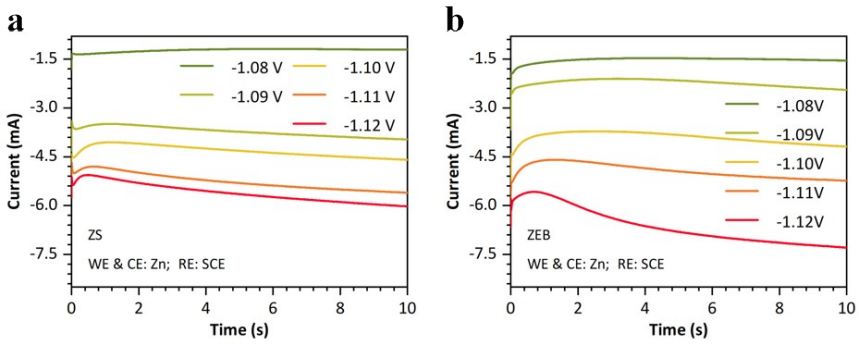

Figure S15. CA curves of zinc nucleation process at different voltages in (a) ZS and (b) ZEB electrolytes.

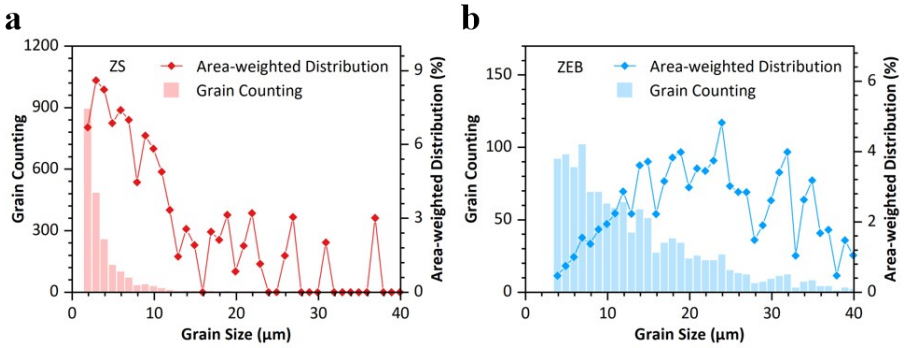

Figure S16. Statistical analysis of zinc grain size obtained from (a) ZS electrolyte and (b) ZEB electrolyte. Grain size is using the equivalent circle diameter method.

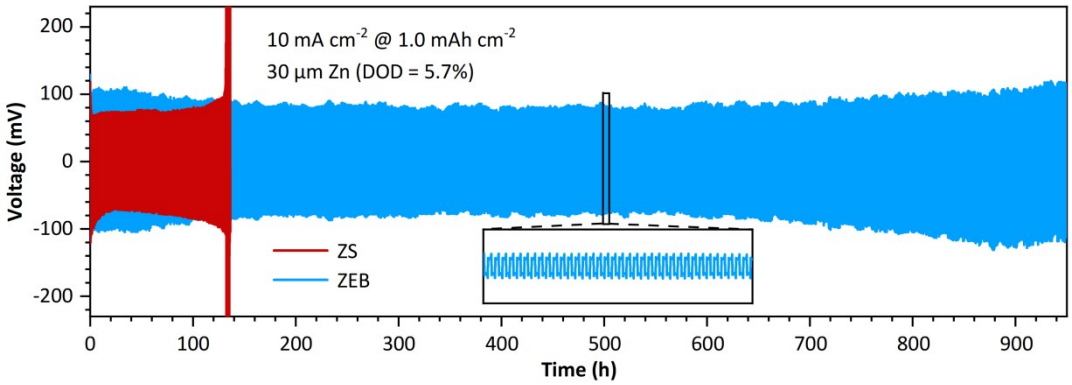

Fig. S17 Cycling performance of Zn||Zn symmetric cells at 10 mA cm^{-2}, 1.0 mAh cm^{-2}.

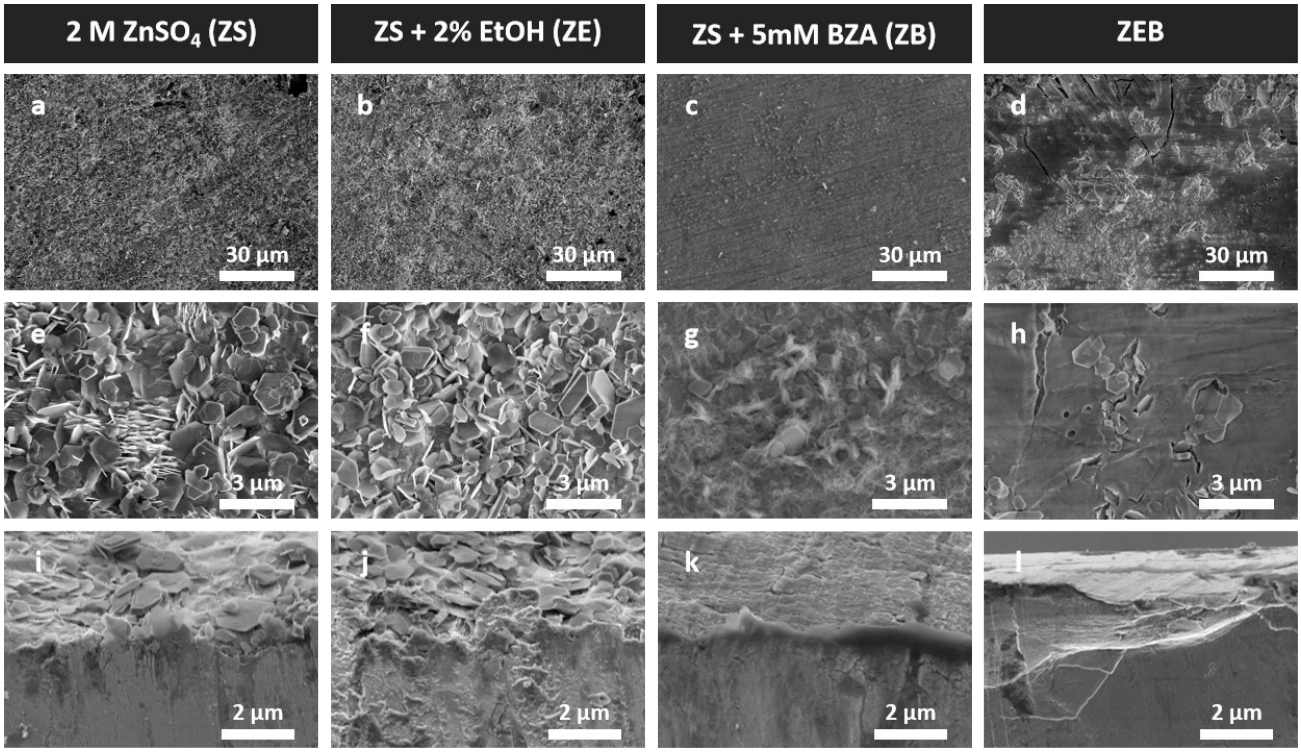

Fig. S18 SEM images of Zn surfaces after 120 h of cycling at 1.0 mA cm^{-2}, 1.0 mAh cm^{-2}.

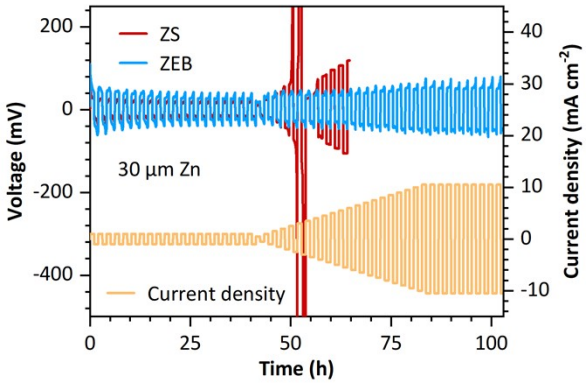

Fig. S19 Critical current density (CCD) test for Zn||Zn (30 µm) symmetrical batteries.

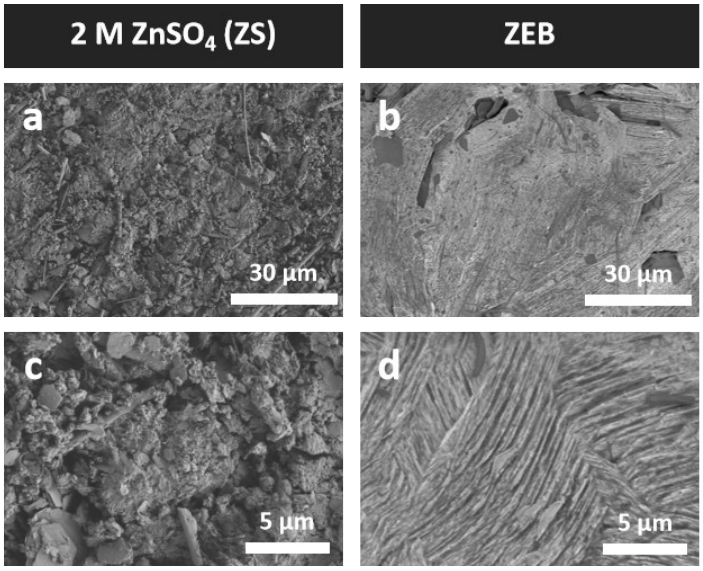

Fig. S20 Scanning electron microscopy (SEM) image of the Zn anode surface after cycling for 120 hours at 10 mA cm^{-2} in the ZEB electrolyte.

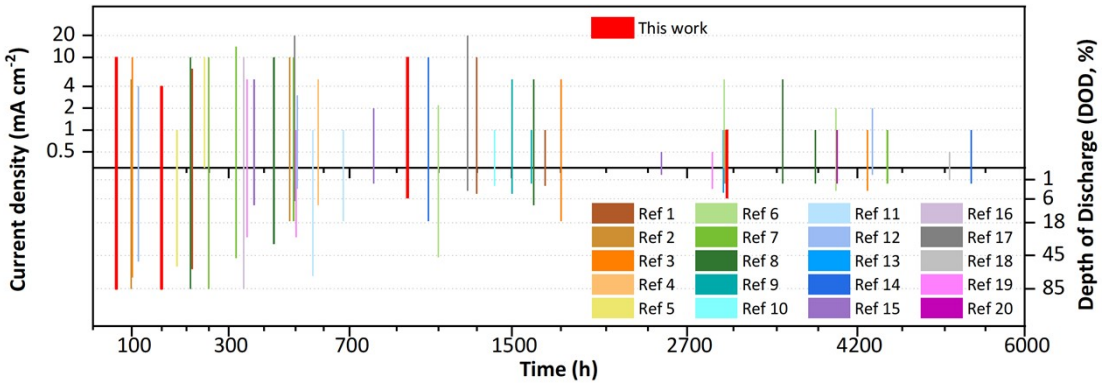

Fig. S21 Comparison of cycle life at different current densities and DOD with recent literature.

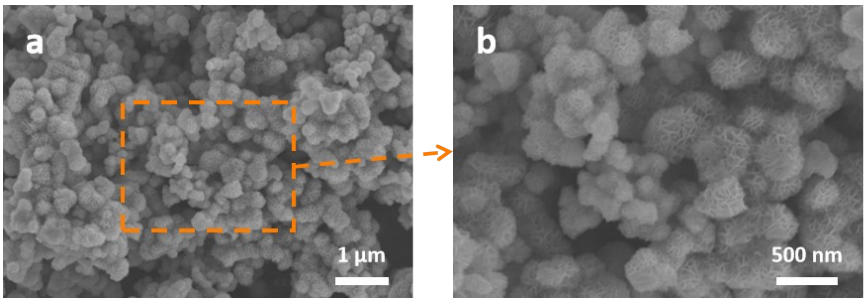

Fig. S22 SEM image of δ−MnO_2.

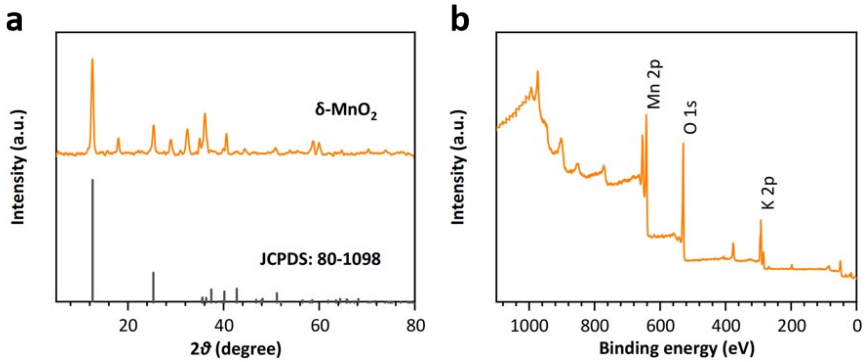

Fig. S23 (a) XRD pattern; (b) XPS spectrum of δ−MnO_2.

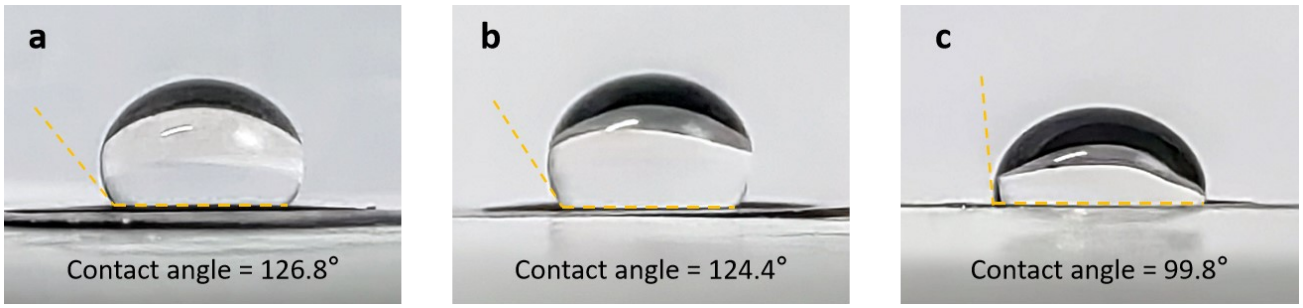

Fig. S24 Contact angles between the δ−MnO_2 cathode sheet and different electrolytes: (a) ZS; (b) ZE; (c) ZEB, the volume of electrolyte is 40 μL.

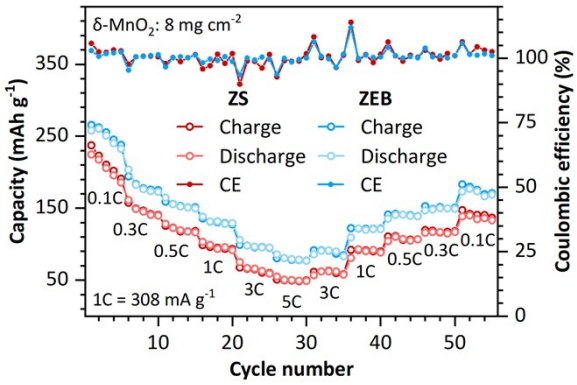

Fig. S25 The rate performance for Zn||δ−MnO_2 full cells with a high cathode mass loading of 8 mg cm^{-2}.

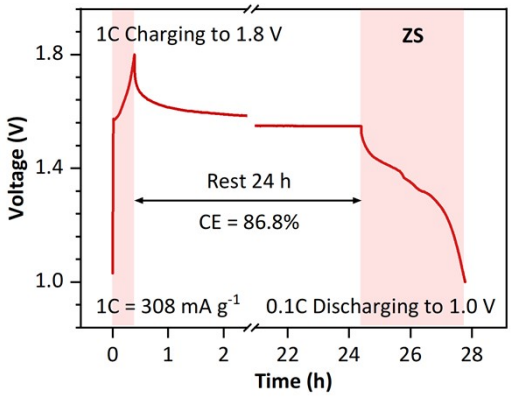

Fig. S26 Self−discharge results for Zn||δ−MnO_2 (8 mg cm^{-2}) full cells using ZS electrolyte.

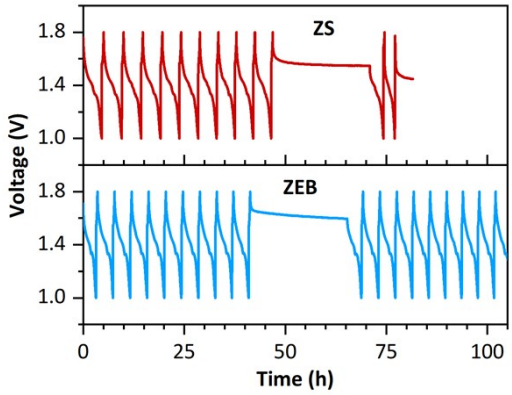

Fig. S27 Voltage-time data for Zn||δ−MnO_2 (8 mg cm^{-2}) full cells used for self−discharge testing (1C charging to 1.8 V and 0.1C discharging to 1.0 V).

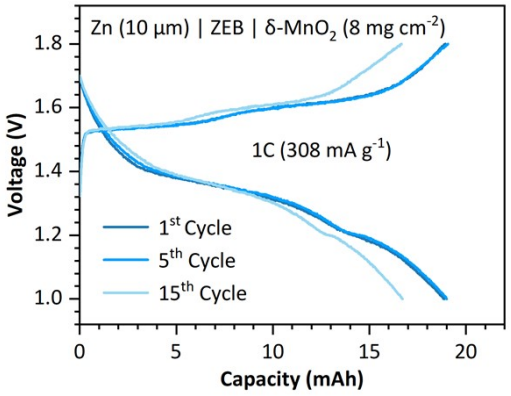

Fig. S28 Voltage-capacity profiles of a 4×4 cm^2 pouch cell at 1C.

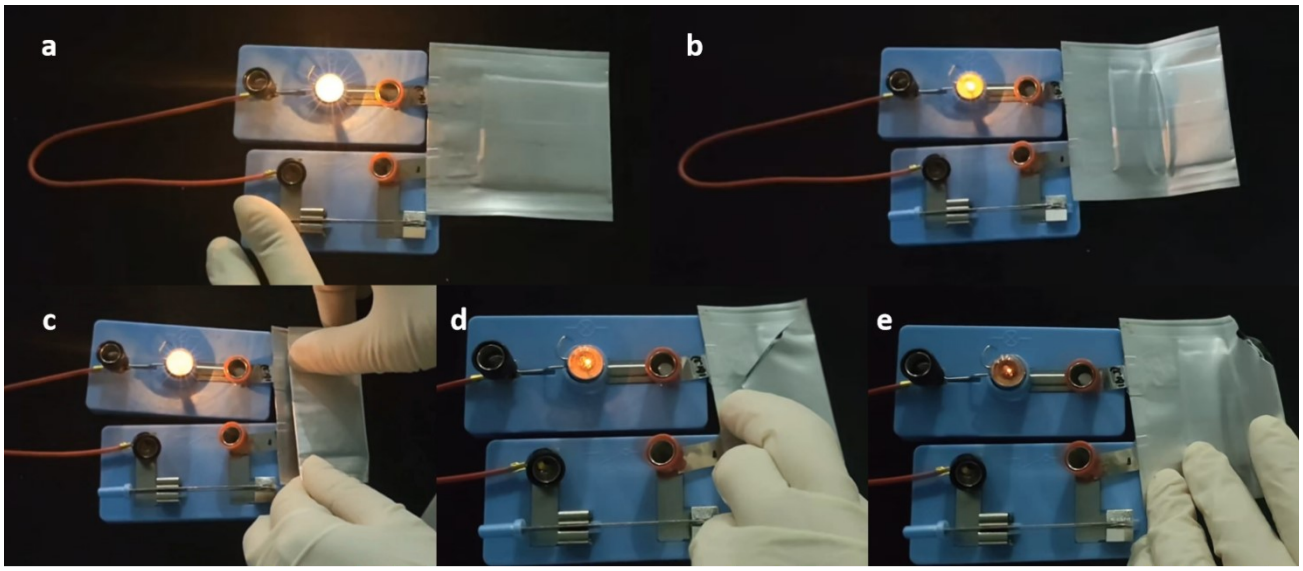

Fig. S29 Schematic diagram of the single-layer pouch cell powering a 1.5 V 0.3 A bulb and undergoing destructive tests. (a) Normal condition; (b) Partial bending; (c) Complete bending; (d) Bending + cutting; (e) Reverse bending after cutting.

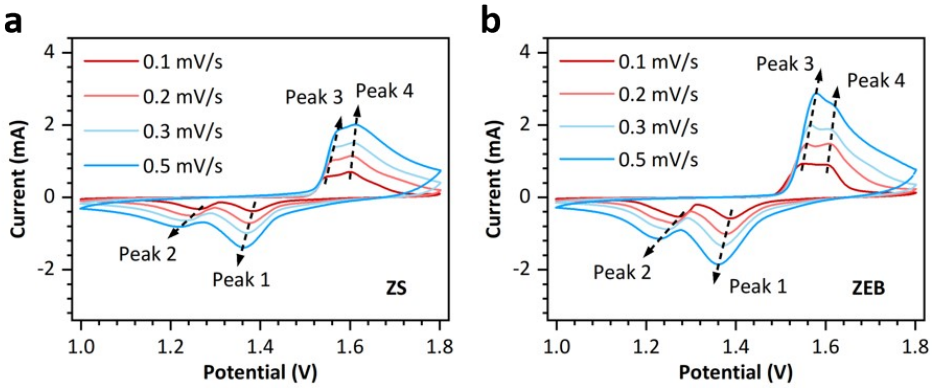

Fig. S30 CV curves at different scan rates for Zn||δ−MnO_2 full cells using (a) ZS; (b) ZEB.

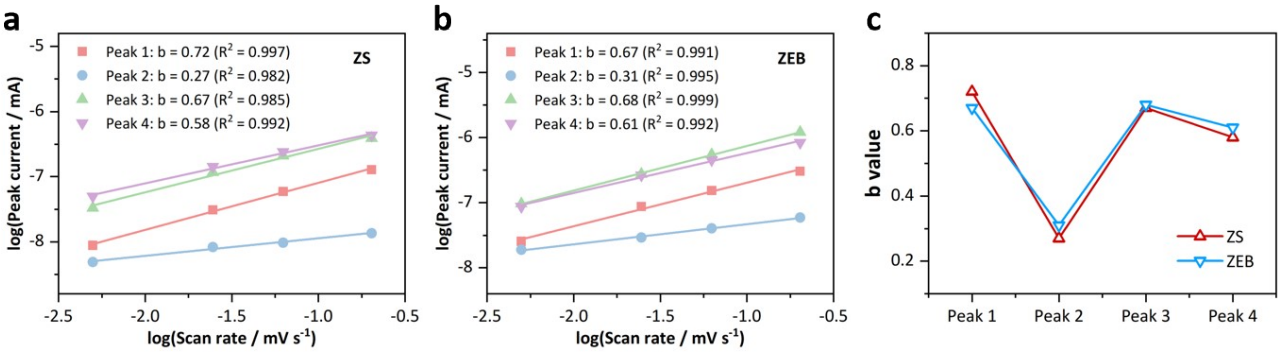

Fig. S31 Logarithmic fitting results of peak current versus scan rate for different peaks in CV curves of Zn||δ−MnO_2 full cells using (a) ZS; (b) ZEB.

Supplementary Tables

Table S1. Unit price of various chemicals in the China market

Reference	Additive	Price (RMB ton^{-1})	Quotation Time	Concentration	Extra Cost* (RMB L^{-1})
This work	EtOH	3500[a]	2026-02-28	0.3 M	0.0674
	BZA	26000[b]	2026-02-26	5 mM	
Ref. 1[16]	18-crown-6	99000[c]	2026-03-28	0.5 M	13.1
Ref. 2[17]	4-dimethylamino-Pyridine (DMAP)	130000[d]	2026-03-10	0.1 M	1.59
Ref. 3[18]	Piperidine-2-carboxylic acid (PPCA)	460000[e]	2026-01	0.1 M	5.94
Ref. 4[19]	Sulfobutyl groups-grafted β-cyclodextrin (SC)	780000[f]	2026-01-10	10 mM	13.3
Ref. 5[20]	Cellobiose (CBS)	80000[g]	2026-01-05	50 mM	1.37
Ref. 6[21]	Citric acid (CA)	5200[c]	2026-03-28	20 mM	0.667
	aspartame (APM)	110000[h]	2026-01-10	20 mM	
Ref. 7[22]	N, N'-methylene-bisacrylamide (MBA)	42000[i]	2026-03-15	30 mM	0.194
Ref. 8[23]	Polyquaternium-6 (P-6)	30000[j]	2026-02-10	8 g L^{-1}	0.240
Ref. 9[24]	Xylo-oligosaccharide (Xos)	50000[k]	2026-01-20	0.2 M	1.52
Ref. 10[25]	EtOH	3500[a]	2026-02-28	20vol%	4.34
Ref. 11[26]	n-Propanol (NPA)	6000[l]	2025-11-06	90vol%	0.552

[a]Nantong Zhonghe Chemical New Material Co., Ltd.; [b]Wuhan Youji Xinrong Chemical Co., Ltd.; [c]Shandong Zhengxing New Material Co., Ltd.; [d]Shandong Mantanghong New Material Co., Ltd.; [e]Wuhan Pushida Biotechnology Co., Ltd.; [f]Shandong Yonghao Biotechnology Co., Ltd.; [g]Shandong Aicai Biotechnology Co., Ltd.; [h]Vitasweet Co., Ltd.; [i]Shandong Xingsheng New Material Co., Ltd.; [j]Shandong Taihe Water Treatment Co., Ltd.; [k]Shandong Longlive Bio-Technology Co., Ltd.; [l]Nantong Runfeng Petrochemical Co., Ltd.;
*Extra Cost (RMB L^{-1}) = 10^{-6} (ton g^{-1}) Price (RMB ton^{-1}) × Concentration (mol L^{-1}) × M (g mol^{-1}); The volume fraction (δ_V) is converted using the material density: 10^3 (cm^3 L^{-1}) × δ_V × ρ (g cm^{-3});

Table S2. Error analysis of desolvation energy calculation

T (K)	σ_T (K)	R_{ct} (Ω)	σ_{Rct} (Ω)	E_a (kJ mol^{-1})	σ_{Ea} (kJ mol^{-1})
298.15	±0.2	1419	30.9		
303.15	±0.2	946.1	35.5		
308.15	±0.2	696.3	16.6	53.65	0.87
313.15	±0.2	503.4	13.6	(ZS)	(ZS)
318.15	±0.2	353.4	10.8		
323.15	±0.2	271.9	12.6		
298.15	±0.2	2142	23.886		
303.15	±0.2	1502	34.969		
308.15	±0.2	1145	27.34	48.04	0.69
313.15	±0.2	863.1	21.184	(ZEB)	(ZEB)
318.15	±0.2	637.8	16.643		
323.15	±0.2	466.7	13.3		

Table S3. The actual CPVC, $CPVC_{max}$ and their ratios of Zn symmetrical batteries

Electrolyte	ZS	ZE	ZEB
CD / mA cm^{-2}	1.0	1.0	1.0
d_{Zn} / μm	30	30	30
t / h	405	795	3000
CPVC / Ah cm^{-3}	135	265	1000
DOD / %	5.7	5.7	5.7
ACE / %	98.2	99.0	99.2
$CPVC_{max}$ / Ah cm^{-3}	613	1104	1380
CPVC:$CPVC_{max}$ / %	22.0	24.0	72.5

*CD is current density; d_{Zn} is thickness of Zn foil; t is test time; CPVC is cumulative electroplating volumetric capacity; DOD is depth of discharge; ACE is average Coulombic efficiency;

Table S4. An overview of relevant literature in 2025

Reference	Additive	d_{Zn}	CD	AC	t	DOD	CN	CPVC
		μm	mA cm^{-2}	mAh cm^{-2}	h	%	times	Ah cm^{-3}
This work	BZA + EtOH (H-C strategy)	30	1.0	1.0	3000	5.70	1500	1000
		30	10.0	1.0	950	5.70	4750	3167
		10	4.0	5.0	150	85.43	60	600
		30	10.0	15.0	78	85.43	26	260
Ref. 1[16]	18-crown-6	80	1.0	1.0	1700	2.14	850	213
		80	0.1	1.0	953	2.14	48	12
		80	10.0	2.0	1300	4.27	3250	1625
		20	7.0	7.0	210	59.80	105	735
Ref. 2[17]	4-dimethylamino-pyridine	100	1.0	1.0	3000	1.71	1500	300
		100	10.0	10.0	480	17.09	240	480
		10	5.0	5.0	100	85.43	50	500
Ref. 3[18]	Piperidine-2-carboxylic acid (PPCA)	50	5.0	5.0	1800	17.09	900	1800
		50	1.0	1.0	4300	3.42	2150	860
		50	10.0	20.6	100	70.39	24	200
		20	10.0	10.0	250	85.43	125	1250
Ref. 4[19]	Sulfobutyl groups-grafted β-cyclodextrin (SC)	50	5.0	2.5	580	8.54	580	580
		50	1.0	1.0	1300	3.42	650	260
		50	10	1.0	480	3.42	2400	960
Ref. 5[27]	Hydrolytic polymaleic anhydride (HPMA)	n/a	0.5	0.5	3500	n/a	1750	n/a
		n/a	5.0	1.0	3000	n/a	7500	n/a
		30	1.0	10.0	180	56.95	9	60
		n/a	10.0	1.0	240	n/a	1200	n/a
Ref. 6[20]	Cellobiose (CBS)	20	2.2	5.5	1100	46.98	220	1210
		50	2.0	1.0	4000	3.42	4000	1600
Ref. 7[21]	Citric acid (CA) + aspartame (APM)	100	1.0	1.0	4500	1.71	2250	450
		100	10.0	10.0	500	17.09	250	500
		50	14.0	14.0	320	47.84	160	896
		50	10.0	25.0	250	85.43	50	500
Ref. 8[28]	Tyrosine (Tyr)	100	1.0	1.0	3800	1.71	1900	380
		100	5.0	1.0	3500	1.71	8750	1750
		20	10.0	10.0	210	85.43	105	1050
		50	10.0	10.0	430	34.17	215	860
		100	5.0	5.0	1630	8.54	815	815
Ref. 9[22]	N, N'-methylene-bisacrylamide (MBA)	100	1.0	1.0	1600	1.71	800	160
		100	5.0	2.5	1500	4.27	1500	750
Ref. 10[23]	Polyquaternium-6	80	1.0	1.0	1400	2.14	700	175
Ref. 11[24]	Xylo-oligosaccharide (Xos)	100	1.0	10.0	675	17.09	34	68
		100	1.0	40.0	560	68.34	7	56
Ref. 12[29]	$Al_2(SO_4)_3$	100	2.0	0.3	4350	0.43	17400	870
		70	3.0	1.2	500	2.93	625	214
		20	4.0	6.0	110	51.26	37	220

Reference	Additive	d_{Zn}	CD	AC	t	DOD	CN	CPVC
		μm	mA cm^{-2}	mAh cm^{-2}	h	%	times	Ah cm^{-3}
Ref. 13[28]	$[BnNEt_3]^+Cl^-$	42.7	1.0	1.0	3000	4.00	1500	702
Ref. 14[29]	Itaconic acid (IA)	100	1.0	1.0	5390	1.71	2695	539
		100	10.0	10.0	1050	17.09	525	1050
Ref. 15[30]	$(NH_4)_3[PMo_{12}O_{40}]$	100	0.5	0.3	2500	0.43	2500	125
		100	2.0	1.0	800	1.71	800	160
		100	5.0	5.0	370	8.54	185	185
Ref. 16[31]	D-glucuronamide (D-Glu)	20	10.0	10.0	340	85.43	170	1700
		n/a	5.0	1.0	3400	n/a	8500	n/a
		n/a	10.0	5.0	1890	n/a	1890	n/a
Ref. 17[32]	Trifluoroacetamide (CNF)	100	20.0	2.0	1250	3.42	6250	2500
		100	20.0	4.0	500	6.83	1250	1000
Ref. 18[33]	1-(2-hydroxyethyl)-1-methylguanidine dihydrogen phosphate (HMDP)	80	0.5	0.5	5150	1.07	2575	322
Ref. 19[34]	Chitosan (CTS) + $InCl_3$ (hybrid additive strategy)	30	0.5	0.5	2900	2.85	1450	483
		30	1.0	5.0	500	28.48	50	167
		30	5.0	5.0	350	28.48	175	583
Ref. 20[35]	Pyrocatechol violet (PV)	100	1.0	1.0	4000	1.71	2000	400
		100	5.0	1.0	1300	1.71	3250	650

*d_{Zn} is thickness of Zn foil; CD is current density; AC is areic capacity; *t* is test time; DOD is depth of discharge; CN is cycle number; CPVC is cumulative electroplating volumetric capacity;

References

[1] T. D. Kühne, M. Iannuzzi, M. D. Ben, V. V. Rybkin, P. Seewald, F. Stein, T. Laino, R. Z. Khaliullin, O. Schütt, F. Schiffmann, D. Golze, J. Wilhelm, S. Chulkov, M. H. Bani-Hashemian, V. Weber, U. Borštnik, M. Taillefumier, A. S. Jakobovits, A. Lazzaro, H. Pabst, T. Müller, R. Schade, M. Guidon, S. Andermatt, N. Holmberg, G. K. Schenter, A. Hehn, A. Bussy, F. Belleflamme, G. Tabacchi, A. Glöß, M. Lass, I. Bethune, C. J. Mundy, C. Plessl, M. Watkins, J. VandeVondele, M. Krack and J. Hutter, *J. Chem. Phys.*, 2020, **152**, 194103.

[2] J. VandeVondele, M. Krack, F. Mohamed, M. Parrinello, T. Chassaing and J. Hutter, *Comput. Phys. Commun.*, 2005, **167**, 103−128.

[3] P. J. Perdew, K. Burke and M. Ernzerhof, *Phys. Rev. Lett.*, 1996, **77**, 3865−3868.

[4] S. Goedecker, M. Teter and J. Hutter, *Phys. Rev. B*, 1996, **54**, 1703−1710.

[5] S. Grimme, J. Antony, S. Ehrlich and H. Krieg, *J. Chem. Phys.*, 2010, **132**, 154104.

[6] S. Grimme, S. Ehrlich and L. Goerigk. *J. Comput. Chem.*, 2011, **32**, 1456.

[7] J. VandeVondele, J. Hutter. J. Chem. Phys. 127, 114105 (2007). Gaussian basis sets for accurate calculations on molecular systems in gas and condensed phases.

[8] H.J. Monkhorst, J.D. Pack, Special points for Brillouin-zone integrations, Phys. Rev. B 13 (12) (1976) 5188.

[9] Gaussian 16, Revision C.02, M. J. Frisch, G. W. Trucks, H. B. Schlegel, G. E. Scuseria, M. A. Robb, J. R. Cheeseman, G. Scalmani, V. Barone, G. A. Petersson, H. Nakatsuji, X. Li, M. Caricato, A. V. Marenich, J. Bloino, B. G. Janesko, R. Gomperts, B. Mennucci, H. P. Hratchian, J. V. Ortiz, A. F. Izmaylov, J. L. Sonnenberg, D. Williams-Young, F. Ding, F. Lipparini, F. Egidi, J. Goings, B. Peng, A. Petrone, T. Henderson, D. Ranasinghe, V. G. Zakrzewski, J. Gao, N. Rega, G. Zheng, W. Liang, M. Hada, M. Ehara, K. Toyota, R. Fukuda, J. Hasegawa, M. Ishida, T. Nakajima, Y. Honda, O. Kitao, H. Nakai, T. Vreven, K. Throssell, J. A. Montgomery, Jr., J. E. Peralta, F. Ogliaro, M. J. Bearpark, J. J. Heyd, E. N. Brothers, K. N. Kudin, V. N. Staroverov, T. A. Keith, R. Kobayashi, J. Normand, K. Raghavachari, A. P. Rendell, J. C. Burant, S. S. Iyengar, J. Tomasi, M. Cossi, J. M. Millam, M. Klene, C. Adamo, R. Cammi, J. W. Ochterski, R. L. Martin, K. Morokuma, O. Farkas, J. B. Foresman and D. J. Fox, Gaussian, Inc., Wallingford CT, 2019.

[10] P. J. Stephens, F. J. Devlin, C. F. Chabalowski and M. J. Frisch, *J. Phys. Chem.*, 1994, **98**, 11623−11627.

[11] W. Humphrey, A. Dalke and K. Schulten, *J. Molecular Graphics*, 1996, **14**, 33−38.

[12] T. Lu and F. Chen, *J. Comput. Chem.*, 2012, **33**, 580−592.

[13] T. Lu, *J. Chem. Phys.*, 2024, **161**, 082503.

[14] J. Zhang and T. Lu, *Phys. Chem. Chem. Phys.*, 2021, **23**, 20323−20328.

[15] H. J. C. Berendsen, D. van der Spoel and R. van Drunen, *Comput. Phys. Commun.*, 1995, **91**, 43-56.

[16] A. Wu, S. Zhang, Q. Li, W. Xue, C. Li, B. Xi, W. Mao, K. Bao and S. Xiong, *Adv. Energy Mater.*, 2025, **15**, 2404450.

[17] S. Han, Y. Zheng, X. Zhang, S. Alshammari, W. Fan, S. Yin, Z. M. El-Bahy, H. K. Thabet, S. Gong, B. Lu, Y. Liu and J. Zhou, *Adv. Mater.*, 2025, **37**, e11814.

[18] Z. Zhen, Z. Liu, Y. Li, H. Huang, X. Peng, L. Chen, L. Xue, P. Xiong and J. Zhu, *Adv. Funct. Mater.*, 2025, **35**, 2509433.

[19] Y. Li, X. Li, X. Peng, X. Yang, F. Kang and L. Dong, *Nano-Micro Lett.*, 2025, **17**, 268.

[20] S. Zhang, S. Huang, W. Chen, Z. Hu, D. H. Min, J. S. Kim, H. Fu, Y. S. Yun, W.-C. Cho, B.-H. Kim, B. Li, C. Li, J. Sun and H. S. Park, *Adv. Funct. Mater.*, 2025, e23753.

[21] T. Xue, Y. Mu, Z. Zhang, J. Guan, J. Qiu, C. Yang, L. Zang and L. Zeng, *Adv. Energy Mater.*, 2025, **15**, 2500674.

[22] D. Chen, X. Ma, W. Xu, C. Yan, P. Lyu, Q. Zhu, H. Yu, Z. Gao and C. Lv, *Exploration*, 2025, **5**, 20240007.

[23] X. Miao, J. Chen, X. Zheng, H. Li and L. Zhang, *Energy Storage Mater.*, 2025, **82**, 104620.

[24] W. Guo, L. Xu, Y. Su, L. Zhao, Y. Ding, Y. Zou, G. Zheng, T. Cheng and J. Sun, *Angew. Chem. Int. Ed.*, 2025, **64**, e202417125.

[25] Z. Tian, H. Liu, M. Cheng, L. Cui, R. Zhang, X. Yang, D. Wu, D. Wang and J. Xia, *ACS Appl. Mater. Interfaces*, 2024, **16**, 21857−21867.

[26] Z. Liu, J. Sun, X. Li, N. Jiang, Y. Zhang, S. Lei, F. Guo, H. Mi, Q. Yang and J. Qiu, *Energy Storage Mater.*, 2025, **83**, 104727.

[27] J. Li, Y. Long, X. Yu, J. Li, N. Li, J. Han, J. Wang and Z. Yang, *Energy Storage Mater.*, 2025, **76**, 104154.

[28] L. Zhang, M. Lin, Z. Yu, Y. Huang, Q. Sun, X. Lu and H. Cheng, *Energy Storage Mater.*, 2025, **75**, 104022.

[29] T. Ji, D. Feng, Z.-H. Huang, Y. Yao, H. Li, Z. Wu, W. Du, H. Pan and T. Ma, *Adv. Energy Mater.*, 2025, **15**, e03628.

[30] Z. Mai, Y. Lin, J. Sun, C. Wang, G. Yang and C. Wang, *Nano-Micro Lett.*, 2025, **17**, 259.

[31] H. Sun, N. Cai, X. Bai, H. Chen, X. He, D. Zhou and L.-Z. Fan, *Adv. Funct. Mater.*, 2025, **35**, 2424398.

[32] Y. Liu, L. Miao, H. Shen, Z. Wang, K. Yao, Y. Hu, J. Sun, S. Hou, J. Zhao and K. Yang, *Adv. Funct. Mater.*, 2025, **35**, 2501968.

[33] L. Zhang, S. Bi, X. Liu, Q. Sun, T. Hu, X. Lua and H. Cheng, *Energy Environ. Sci.*, 2025, **18**, 7555-7567.

[34] S. Li, X. Chen, J. Zhao, Y. Zhang, K. Zhang, K. Wang, J. Shen, P. Lv, Y. Jia and Y. Bai, *ACS Energy Lett.*, 2025, **10**, 1642-1653.

[35] H. Tong, J. Li, M. Chuai, Y. Sun, Z. Yang, Y. Su, X. Nie, S. Deng, M. Wu and G. Chai, *Energy Storage Mater.*, 2025, **82**, 104609.

[36] J. Song, Z. Ren, Z. Chen, S. Zhang, Z. Yu, J. Cheng and B. Wang, *Energy Storage Mater.*, 2025, **81**, 104523.

[37] W. Liang, D. Li, R. Zhong, S. Tao, Y. Zhu, W. Tan, R. Xu, Y. Yuan, I. Zhitomirsky and J. Lu, *Adv. Funct. Mater.*, 2025, **35**, 2504195.